Available online at www.sciencedirect.com
SCIENCE DIRECT®
International Journal of Mass Spectrometry 243 (2005) 141–149
International Journal of Mass Spectrometry
www.elsevier.com/locate/ijms

A laminar and turbulent ion flow reactor for studying ion/molecule reactions at variable pressures and temperatures

V. Catoire*, E. Michel, C. Guimbaud, D. Labonnette, G. Poulet

Laboratoire de Physique et Chimie de l'Environnement, CNRS, Université d'Orléans (UMR 6115), 3A Avenue de la Recherche Scientifique, 45071 Orléans Cedex 2, France

Received 21 December 2004; accepted 7 February 2005
Available online 7 March 2005

Abstract

A laboratory ion flow reactor operating under wide ranges of temperatures (213–373 K) and pressures (1–50 hPa) has been set up. This will allow for the potential detection of a variety of atmospheric trace gases to be measured by chemical ionization mass spectrometry. Flow dynamics of the reactor has been characterized in detail in order to extract reliable kinetic data and ion/molecule reactions. Direct comparison between the average ion flow velocity and the carrier gas flow velocity has been achieved experimentally under laminar and turbulent flow conditions. To validate this new setup, the reaction of SF_6^- ions with SO_2 molecules has been studied giving kinetic and mechanistic results in excellent agreement with previous studies conducted at room temperature at low (<2 hPa) and very high pressures (>30 hPa). Consistent data have also been obtained under intermediate pressure conditions and at other temperatures, which definitely establishes $SF_6^- + SO_2$ as a reference reaction for future fast flow reactor or reaction kinetics validation.

Keywords: Turbulent flow reactor; CIMS; Ion/molecule reaction; SF_6^- ion; SO_2

1. Introduction

Chemical ionization mass spectrometry (CIMS) is more and more used as a fast and in situ detection method for trace gases in the atmosphere. This method is based on reactions of ions with the trace gases, which form specific product ions detected by mass spectrometry. This detection generally occurs in two pressure regimes, either at high pressure (around 1 atm = 1013.25 hPa) in the so-called atmospheric pressure chemical ionization mass spectrometry (APCI-MS), or at low pressure (around 1 hPa). APCI method provides a better sensitivity but requires very short reaction times (a few microseconds) in order to reduce the reaction advancement, which simplifies data analysis [1]. Practically, in APCI-MS instruments, the chemical ionization regions are defined by the use of a dc point-to-plane discharge (with typical reaction length of few mm within a field of a few kV cm^{-1}). In such chemical ionization regions, many parameters are not well defined, such as the reaction time, the effective temperature or the kinetic parameters of the ion-molecule reactions. As a consequence, the APCI-MS method requires calibration standards for the quantitative detection of trace gases. In contrast, in the low pressure chemical ionization mass spectrometry method, longer reaction times (a few milliseconds) are obtained using flow reactors or electrostatic drift tubes. In this case, the kinetic parameters of the ion-molecule reactions are well defined, preventing any need of calibration standards for the quantitative detection of trace gases. As an example, for the detection of organic molecules, proton transfer reaction (PTR-MS) is often used, with H_3O^+ reactant ions formed in a drift tube from higher hydrated clusters $H_3O^+(H_2O)_{n=1–5}$ [2–4]. However, PTR-MS is unable to distinguish between molecules with the same molecular mass, which is common for organics. Another low pressure method using the selected ion flow tube (SIFT) also allows for a single type of ions to react with the trace molecules [5]. These low pressure methods lead to simple spectra, but may be of lower sensitivity

* Corresponding author. Tel.: +33 238494915; fax: +33 238494672.
E-mail address: valery.catoire@univ-orleans.fr (V. Catoire).

1387-3806/$ – see front matter © 2005 Elsevier B.V. All rights reserved.
doi:10.1016/j.ijms.2005.02.003

than APCI-MS and restricted to molecules with significant reactivity at low pressure.

Alternative methods with the advantages of high sensitivity and virtually no calibration are based on the use of a high pressure flow reactor. They have been successfully employed for measuring inorganic trace compounds such as OH, HNO_3, H_2SO_4 and SO_2 and a few organics such as acetone and methyl cyanide [6–17]. In such methods, the kinetics and potentially complex mechanisms of the corresponding ion/molecule reactions must be well characterized from laboratory studies performed under the same experimental conditions as those of in situ measurements, which is not often the case at present. In fact, calibration standards are sometimes used even in these methods using high pressure flow reactors. Therefore, in order to be able to measure a large variety of trace compounds with very good sensitivity and accuracy, it is necessary to extend the kinetic database in a wide range of pressure and temperature. Indeed, ion/molecule collision theory [18–20] is not always applicable, and discrepancy may exist between theoretical and experimental rate constants, suggesting either that the high pressure limit is not reached or that complex mechanism occurs. Using the turbulent flow approach similar to that used for kinetic studies of neutral species [21], only one group has conducted very high-pressure (>30 hPa) experiments of ion/molecule reactions in a flow reactor [22].

In our laboratory, studies of ion/molecule reactions have already been conducted with a flow reactor operating essentially at ambient temperature and low pressures [23]. In this paper, a new variable temperature flow reactor is presented, allowing for kinetic measurements under both conditions of laminar and turbulent flows, in a pressure range (1–50 hPa) which is intermediate between the low pressures used in classical laminar ion flow reactors and the very high pressure used in the so far unique turbulent ion flow reactor [22]. The data obtained in this pressure range can be easily extrapolated to higher pressures relevant for atmospheric measurements after checking that they do not present pressure dependence in the upper part of the range explored. If they do present pressure dependence, theoretical extrapolation of the fall-off regime to high pressure limit can be made using the experimental data obtained at lower pressures [24,25]. Since this turbulent flow reactor method is not routinely used, the flow regimes of the new setup have been characterized in detail, in order to extract reliable kinetic data. Comparative measurements of the carrier gas flow velocity and of the ion flow velocity have been performed. Finally, the data obtained in wide ranges of pressure and temperature are reported for the reaction of SF_6^- ions with SO_2 molecules, for which kinetics is very well established at room temperature. This enables the testing of capabilities of the new setup and the validation of the method.

2. Experimental method

2.1. Apparatus and reactants

The new apparatus is schematically presented in Fig. 1. It consists of two main parts: the flow reactor including the injection system for neutral molecules and the ion sources, and the detection system comprising three differentially pumped chambers where the ions were sampled, focused and mass analyzed. The new ion flow reactor is a triple jacketed stainless steel tube. Ion/molecule reactions took place in the inner tube (88 cm long × 2.3 cm i.d.). N_2 carrier gas flows of 2–100 STP $dm^3\ min^{-1}$ (standard temperature and pressure: $T = 273.15$ K, $P = 1013.25$ hPa) coming from a liquid nitrogen tank (Air Liquide, purity > 99.999%) were maintained by a 250 $m^3\ h^{-1}$ rotary pump and resulted in pressures of 1–50 hPa that also depend on the throttling of the gate located between the flow tube and the rotary pump. Flows were monitored using MKS mass flow meters, which are periodically calibrated. Higher pressures have not been tested, due to the prohibitive cost of larger flows of high purity N_2 and due to too low ion signals detected. Pressure was measured at the entrance of the tube by two calibrated MKS capacitance gauges P_1 (0–100 and 0–13 hPa) and at the downstream end by one MKS capacitance gauge P_2 (0–100 hPa). The injection system for the neutral reactants consists of a concentric 6.35 mm o.d. and 4 mm i.d. movable line. This injector is terminated by a closed spherical tip with six apertures pointing radially. The neutral reactant flow was thus directed perpendicularly to the main flow direction, which accelerates the reactant mixing.

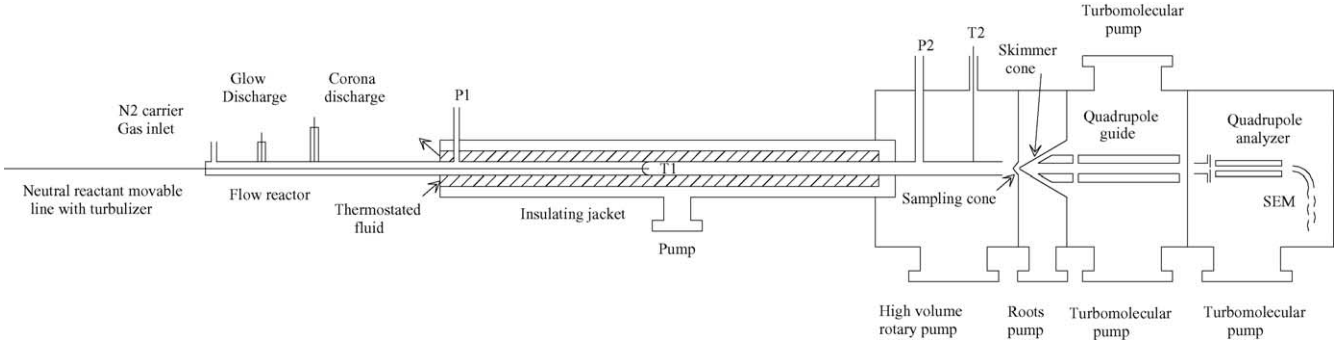

Fig. 1. Overview of the variable pressure and temperature ion flow reactor coupled to the mass detection system.

In addition, when operating under turbulent flow regime conditions, a fan shaped turbulizer was placed 1 cm upstream of the injector tip in order to reduce the delay of homogeneous mixing between neutral and ion reactants, as shown by Seeley et al. [21]. A thermostated fluid circulated through the intermediate jacket, enabling to set temperatures in the reactor in the range (213–373 K). The temperature of the flowing gas was measured using two chromel–alumel thermocouples. One (T_1) was placed at the movable injector tip and the other (T_2) at the downstream end of the reactor just before the detection system. The carrier gas was precooled or preheated before being introduced into the flow tube by passing through a cooper spiral immersed in a liquid nitrogen bath or heated by an electric resistor wire. The injector containing the neutral reactant/N_2 mixture was also precooled by dry ice or preheated by an electric resistor wire. The downstream end of the reactor was not thermostated but the temperature of the gas was maintained by dry ice or by a heating wire. The amount of precooling (or preheating) and the position of the movable injector were adjusted so that the temperature measured at the injector tip matched that measured at the downstream end of the reactor. Vacuum was maintained in the third jacket for thermal insulation.

In the present validation study, SF_6^- ions have been used. They were generated by electron attachment to flowing (10^{-3} STP dm^3 min^{-1}) SF_6 parent gas (Air Liquide, purity > 99.97%). The electrons were produced from argon ionization in two discharges. One discharge (the glow discharge) was produced by a permanent voltage (typically 600 V and 0.3 mA) applied between a molybdenum needle and a stainless steel capillary tube containing flowing argon (typically 1 STP dm^3 min^{-1}), and the other (called corona discharge) was produced by a permanent voltage (typically 360 V and 0.3–5 mA) applied between a tungsten needle and a stainless steel cylinder containing flowing argon (typically 1.5 STP dm^3 min^{-1}). SF_6 was introduced by an inlet perpendicular to the flow tube and located 8.4 cm downstream from the nearest ion source (corona discharge), a distance sufficient for most of the electrons to be thermalized. Together with SF_6^- ions (m = 146 and 148 amu), SF_5^- ions (127 and 129 amu) were generated in traces (<2% SF_6^-). At the highest pressure used in the present study (30.2 hPa), SF_6^- breakup during sampling, which would have led to an increase of SF_5^- signal, did not occur. This phenomenon was observed by Arnold et al. [22] at higher pressure (>200 hPa). The neutral reactant was introduced at variable distances downstream of the corona discharge (73.2–26.0 cm) and glow discharge (81.6–34.4 cm). This results in reaction distances in the range 33.0–81.2 cm. In the present study, the neutral reactant is sulfur dioxide (Air Liquide, purity > 99.9%), obtained from a gas cylinder, used without further purification and diluted with N_2 (Air Liquide, purity > 99.9999%) in a bulb with mole fractions of (1.07–20.47) × 10^{-4}. SO_2/N_2 mixtures flows of (0.94–403.6) × 10^{-3} STP dm^3 min^{-1} into the reactor were deduced by monitoring pressure variations in the bulb as a function of time at a constant temperature.

The detection system has been already described in detail [23,26], and is thus briefly presented with the parts modified. A small fraction of the total flow was sampled through the 0.2 mm i.d. orifice of a conical electrode typically biased at 5 V. The first chamber was pumped by a roots blower system (480 m^3 h^{-1}), giving pressures lower than 10^{-1} hPa. The sampled ions were then focused over a 4 mm length path and skimmed by the 1.5 mm i.d. orifice of a conical electrode (typically 10 V) through the second chamber containing electrostatic lenses (50 V) and a quadrupole guide (operating in radiofrequency mode only, and with a field axis of 30 V). This second stage was pumped by two turbomolecular pumps (with a total capacity of 2000 m^3 h^{-1}), resulting in pressures lower than 10^{-4} hPa. Ions enter the third chamber through the 3 mm i.d. orifice of an inlet plate (20 V) where they were focused by electrostatic lenses (30 and 180 V) and were selected by a quadrupole mass analyzer (with a field axis of 60 V) and detected after a 90° deflection by a dynode secondary electron multiplier (SEM) operating in the pulse counting mode. This third chamber was pumped by a turbomolecular pump (830 m^3 h^{-1}), resulting in pressures lower than 10^{-6} hPa.

2.2. Flow dynamics and kinetic analysis

The extraction of reliable kinetic data requires a good characterization of the flow dynamics. The carrier gas (N_2) in very large excess over the reactants determines the nature of the flow. Over the pressure and flow velocity ranges used, the flow is viscous and incompressible, according to the values of the Knudsen number (≪0.01) and Mach number (≪0.3). The dimensionless Reynolds number defining the flow regime is, in the case of tubular flow,

$$Re = \frac{2a\rho P v_b}{\eta} \quad (1)$$

where a (=0.0115 m) is the flow tube radius, ρ (kg m^{-3} hPa^{-1}) is the pressure-independent density, P (hPa) is the pressure in the flow tube, v_b (m s^{-1}) is the average flow velocity of the carrier gas or bulk flow velocity, and η (kg m^{-1} s^{-1}) is the viscosity of the carrier gas [27]. Given that

$$v_b = \frac{Q}{\pi a^2} \quad (2)$$

with Q (m^3 s^{-1}) as the total flow rate of the gases, the Reynolds number may be rewritten as a function of parameters that can be varied in the experiments, i.e. the total flow rate at standard temperature and pressure Q^0 (STP m^3 s^{-1}), and the temperature T (K) of the flow tube:

$$Re = \frac{2\rho P^0 Q^0 T}{\pi a \eta T^0} \quad (3)$$

Experiments were generally performed in two kinds of flow regimes: at low flow rates under laminar flow conditions with Re < 300, and at higher flow rates under turbulent flow conditions with Re > 3300. The transition region, empirically de-

fined by *Re* ranging from 1000 to 2300 [28], may be characterized by fluctuations of the flow velocity and reactant concentration inhomogeneity, which is inappropriate for obtaining reproducible results [29]. The few experiments we have performed in this region resulted in a 50% scattering for the kinetic results.

2.2.1. Laminar flow regime

In laminar flow regime, a parabolic radial profile develops for the carrier gas flow velocity within a distance named the entrance length, $\ell \approx 0.115a\,Re$ [28], which is less than 40 cm under our usual experimental conditions ($Re < 300$). Neglecting the perturbation of small ion flow addition to the carrier gas and because the neutral injector tip is located at least 43 cm downstream of the carrier gas entrance, the velocity $v(r)$ of the carrier gas has thus approximately a parabolic profile when arriving in the reaction zone. This is theoretically expressed as

$$v(r) = 2v_b\left(1 - \frac{r^2}{a^2}\right) \tag{4}$$

where r is the radial coordinate, which gives a maximum $v_{max} = 2v_b$ on the axis of the flow tube. In this case, Poiseuille law giving the pressure gradient ΔP between two points separated by a distance L may be applied:

$$\Delta P = \frac{8L\eta v_b}{a^2} \tag{5}$$

This was checked by measurements between the upstream and downstream located pressure gauges, which were in very good agreement with this equation. Consequently, the pressure of the midpoint of the reaction zone, taken as the pressure of the reaction, was calculated using this equation. In addition, under turbulent flow regime conditions, Blasius formula was applied:

$$\Delta P = 0.066515\mathrm{L}\left(\frac{\eta\rho^3 v_b^7}{a^5}\right)^{1/4} \tag{6}$$

Variations of ρ and η with temperature were taken into account [27].

Under steady-state flow conditions in the reactor, the transport and reaction of reactant ions $A^{\pm}$ with neutral molecules B in excess is described by the three-dimensional continuity equation [30]:

$$v_i(r)\frac{\partial[A^{\pm}]}{\partial z} = \frac{D_A}{r}\frac{\partial}{\partial r}\left(r\frac{\partial[A^{\pm}]}{\partial r}\right) + D_A\frac{\partial^2[A^{\pm}]}{\partial z^2} - k[B][A^{\pm}] \tag{7}$$

where z is the axial coordinate and $v_i(r)$ is the ion flow velocity a priori radially dependent. The term $(D_A/r)(\partial/\partial r)(r(\partial[A^{\pm}]/\partial r))$ represents the ion loss by radial diffusion with D_A as the diffusion coefficient of $A^{\pm}$ in the carrier gas, and the term $k[B][A^{\pm}]$ is the ion loss by chemical reaction with k as the second-order rate constant. Losses of ions along the flow tube induce an axial concentration gradient and thus, potentially, axial diffusion represented by the term $D_A(\partial^2[A^{\pm}]/\partial z^2)$. Using low pressures (<1 hPa) of He as a carrier gas, Ferguson et al. [30] and Adams et al. [31] have shown that the measured rate constant should be corrected for this axial diffusion by a few percent, depending on $(D_A/v_i a)^2$. In our study, the ion flow velocity and the flow tube radius are of the same order of magnitude as in their experiments. The correction has been therefore found to be negligible (<0.1%) under our typical conditions using higher N_2 pressures, since the diffusion coefficient is inversely proportional to pressure and at least five times lower for ions diffusing in N_2 than in He [32]. In the absence of axial diffusion term, the continuity equation (Eq. (7)) has been solved by numerical and analytical methods for laminar flows [30,31,33]. The solution is of the form

$$[A^{\pm}]_z = [A^{\pm}]_e\, e^{\{-((\Delta D_A/a^2)+\Gamma k[B])(z/v_b)\}} \tag{8}$$

where $[A^{\pm}]_e$ and $[A^{\pm}]_z$ are the concentrations of $A^{\pm}$ at the entrance point of B (the neutral injector tip in our case) and at the sampling cone, respectively, z is the reaction distance, Δ is a constant and $\Gamma = v_b/v_i$, with v_i as the radially averaged ion flow velocity [34]. The analysis thus requires the knowledge of v_i. It is known that a large radial concentration gradient arises for the ions because of losses at the reactor walls at every collision. Radial molecular diffusion is not efficient enough to maintain a uniform radial ion distribution. The ion radial concentration profile superimposed on the parabolic velocity profile of the carrier gas $v(r)$ causes the average ion flow velocity v_i to be higher than the average carrier gas flow velocity v_b. Particularly depending on the form of the ion concentration gradient, the ratio v_i/v_b has been theoretically found between 1.33 and 1.63 at room temperature at low He pressure [30,31]. Experimental v_i/v_b ratios reported are in the range 0.8–1.7 at room temperature [30,34-36], also depending on the radius and roughness of the flow tube, on the pressure, and on the flow velocity and nature of the carrier gas. The ion velocity v_i was determined by disturbing the ion flow by an electric pulse and synchronously recording the ion arrival time on the SEM detector by a multichannel analyzer. The electric pulse was applied on a small metallic rod, in place of the pressure gauge P_1, entering perpendicularly the flow tube at a known (87.2 cm) distance from the sampling cone. The time spent by the ions to go through the detection region is negligible according to the calculation of their velocity. This one is essentially due to the electric fields present in the three differentially pumped chambers. Using the typical electric fields and pressures mentioned in Section 2 and reduced mobilities estimated to be about 2 $cm^2\,V^{-1}\,s^{-1}$ for all ions in N_2 [32,37] led to a total time of a few microseconds, i.e. much lower than the few milliseconds taken to travel through the flow tube. This has also been verified experimentally by simultaneously measuring the arrival times on the sampling cone and on the SEM without observing any

difference. Regular measurements were made before and after kinetic experiments, leading to typical values of about 130 m s^{-1} with statistical uncertainties of 10% (2σ) at room temperature whatever the flow dynamics regime.

2.2.2. Turbulent flow regime

As the total flow rate Q is increased, the flow becomes turbulent, for Reynolds number at least above 2300. In contrast to laminar flow regime in which mixing occurs via molecular diffusion only, turbulent mixing comprises processes realized at different scales, i.e. macro-, meso- and micro-scales. Chemical reaction is a molecular-level process and thus affected only by micromixing. For gases, macro- and mesomixing are the limiting steps for the rate of turbulent diffusion [38]. Using a fan-shaped turbulizer, Seeley et al. [21] visually observed macromixing in a few centimeters, which therefore implies the occurrence of fast mixing of the reactants at the microscopic level. This turbulent mixing flattens the radial velocity profile of the carrier gas, which is no more parabolic. The carrier gas flow velocity $v(r)$ is constant within the central part of the tube and approaches the bulk flow velocity value v_b. The ion flow velocity should follow the same behaviour, with no radial dependence. By using a Pitot tube, the carrier gas flow velocity $v(r)$ was measured as a function of the radius in order to confirm the development of turbulence and to compare it with v_i. The Pitot tube was located in place of the pressure gauge P_1, with no possibility of axial motion due to the design of the triple jacketed flow reactor. The distance (10.8 cm) between the injector equipped with the turbulizer and the Pitot tube was sufficient to allow for development of turbulence, as noted by previous workers [21,39], and verified in the present study (see Section 3.2). The probe consists of two stainless steel concentric tubes of a total 2.5 mm o.d. The inner one with a 0.8 mm i.d. orifice parallel to the main flow allows measuring the total pressure, and the outer one with three 0.3 mm i.d. holes perpendicular to the flow gives the static pressure. This set could be moved radially and the two pressures were measured alternately by the same MKS pressure gauge (of 10 hPa full scale), from which the carrier gas velocity $v(r)$ was deduced.

Under turbulent flow conditions, the continuity equation (Eq. (7)) is still valid, with the molecular diffusion coefficient D_A replaced by an effective diffusion coefficient D_{effA} incorporating mixing at the different scales. Neglecting again the axial diffusion term, the solution is of the type of Eq. (8), and again v_i needs to be determined. Kinetics analysis is thus similar for laminar and turbulent flows. In the present case, $[B] = [SO_2] = 3.4 \times 10^9$ to 6.0×10^{11} molecules cm^{-3}, much larger than $[A^-] = [SF_6^-] < 10^8$ ions cm^{-3}, estimated by measuring the ion current on the sampling cone. The rate constant k was then generally determined by varying $[SO_2]$ at a fixed reaction distance z, using the pseudo-first-order kinetics relationship inferred from Eq. (8):

$$\ln\left(\frac{[SF_6^-]_z}{[SF_6^-]_{z,0}}\right) = -k[SO_2]\frac{z}{v_i} \quad (9)$$

where $[SF_6^-]_z$ and $[SF_6^-]_{z,0}$ are the ion count rates collected on the SEM in the presence and absence of sulphur dioxide, respectively, and z/v_i defines the reaction time.

3. Results and discussion

3.1. Flow dynamics

At low Reynolds numbers ($\leq$1000) characteristic of laminar flow regime (corresponding to $P < 7$ hPa), an attempt of measuring the flow velocity radial profile of the carrier gas at room temperature has been made by using the Pitot tube. The typical parabolic profile could not be observed, due to limitations of this technique at low *Re* [21]. At higher *Re* corresponding to the transition flow regime, large fluctuations of the flow velocity at $|r| > 0.1$ cm did not allow measuring reproducible radial profiles either. However reproducible $v(r)/v_b$ values near the axis of the tube ($-0.1 \leq r \leq +0.1$ cm) were obtained for *Re* between 290 and 2000, decreasing from 1.7 to 1.1, as shown in Fig. 2. From the trend observed and taking into account the potential errors and the slight eccentricity of the measurement positions, it is anticipated that at lower *Re*, $v(r)/v_b$ approaches the maximum value (2.0) characteristic of laminar flow at the center of the tube. The decay characterizes the transition regime, in which radial mixing takes more and more importance up to complete homogenization by turbulence. At $Re \geq 2600$ (corresponding to $P > 15$ hPa), the radial velocity profile was reproducible and flat over almost the flow tube diameter ($-0.9 \leq r \leq +0.9$ cm). In addition, the $v(r)/v_b$ ratio was found to be equal to (1.0 ± 0.1), where the quoted uncertainty includes only experimental scatter (2σ). These two results are evidence of occurrence

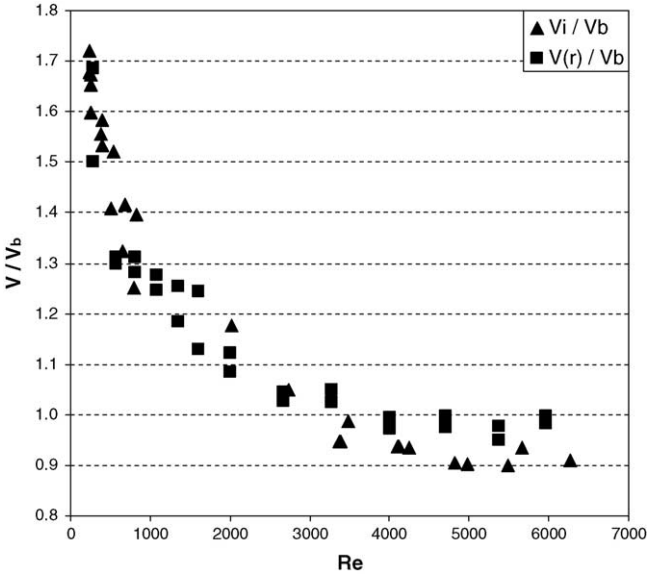

Fig. 2. Comparison of the ratios of the average ion velocity to bulk flow velocity (v_i/v_b) and the carrier gas flow velocity (at $-0.1 \leq r \leq +0.1$ cm) to bulk flow velocity ($v(r)/v_b$) as a function of Reynolds number.

of the turbulence in the flow reactor at these *Re* values. Fig. 2 displays all the results for $v(r)/v_b$ (with $-0.1 \leq r \leq +0.1$ cm) as a function of *Re* comprised between 290 and 6000.

The ratio v_i/v_b at room temperature was also measured and found to decrease from 1.7 to 0.9 as a function of Reynolds numbers comprised between 240 and 6300, as shown in Fig. 2. Typical v_i/v_b values were 1.6 and 1.0 for most of our experiments conducted at $Re = 260$ (at 2.1 hPa) and $Re = 3400$ (at 18.6 hPa), respectively. No dependence in temperature was observed, suggesting that ions and carrier gas have similar flow dynamics behaviours with temperature. Under laminar flow conditions, the v_i/v_b values are almost equal to $v(r)/v_b$, with $-0.1 \leq r \leq +0.1$, which shows that the great majority of ions collected on the sampling cone are those having flown near the flow tube axis, and thus confirming the interpretation of previous experimental results [31]. The highest values not strictly equal to the maximum (2.0) corresponding to the center of the flow tube, recall that v_i is an average velocity with some ions located out of the axis. Under turbulent flow conditions, for $Re > 2600$ according to the Pitot tube experiments, v_i/v_b approaches the asymptotical value 0.9. In theory, this ratio may not lower less than 1.0, but given the associated global uncertainties (10% for v_i mainly originating from the ill-defined shape of the ion current signal generated by the electric pulse, and 10% of potential systematic errors for v_b originating from uncertainties in pressure and volumetric flow), the difference is not significant, and thus the systematic shift observed between experimental v_i/v_b and $v(r)/v_b$ (=1.0 ± 0.1) values in turbulent flow regime (see Fig. 2) is not significant either.

3.2. Kinetic study

The rate constant of the reaction

$$SF_6^- + SO_2 \rightarrow \text{ products} \quad (10)$$

was determined under various experimental conditions. It has been extracted from plots of relative logarithmic decay of SF_6^- signal versus SO_2 concentration (Eq. (9)), as illustrated for example in Fig. 3. For extents of reaction corresponding to $[SF_6^-]/[SF_6^-]_0$ ratios between 99% and 6%, linearity was excellent ($R^2 > 0.99$) and zero intercepts were always null within statistical uncertainties (2σ). This indicates that primary chemistry is independent of the range of SF_6^- consumption, i.e. reaction is total and SF_6^- chemically disappears only by reaction with SO_2. The reaction distance has been varied from 35.5 to 81.2 cm with no systematic dependence for the rate constant values whatever the flow regime. The delay for homogeneous mixing of the reactants, usually referred to as 'inlet effect' or 'end correction', is therefore negligible with respect to the reaction time comprised between 2.7 and 6.4 ms (at room temperature). Taking a maximum of 10% error for the rate constant value due to inlet effect at the lowest reaction distance, this corresponds to a few centimeters for homogenization in laminar flow regime,

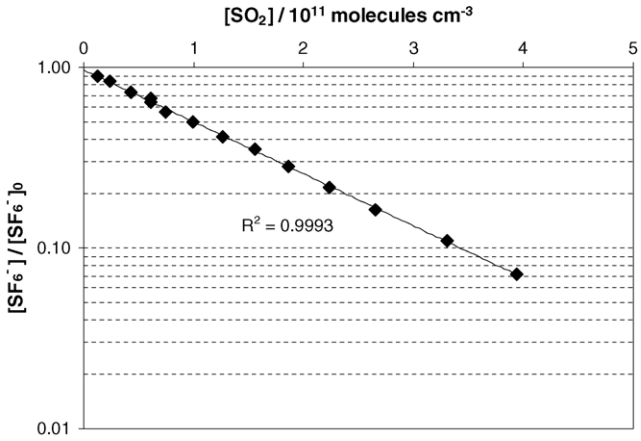

Fig. 3. Example (298 K, 18.6 hPa) of relative logarithmic decay of SF_6^- ion count rate as a function of SO_2 concentration. A linear least-squares fit gives a slope from which the reaction rate constant is derived using Eq. (9) (see text).

as well as in turbulent regime, in agreement with previous studies [21,39]. In turbulent flow regime, the fan-shaped turbulizer is thus efficient for reducing the mixing delay. This was also confirmed by performing experiments without it, in which the rate constant value was found to decrease by 30%. This less consumption of the reactant ion when non-uniform distribution of the neutral reactant takes importance has been also observed in other works under laminar flow conditions, in which inlet effects have been evaluated [30,36]. Under laminar flow conditions however, the presence of the turbulizer was not needed and even led to rate constants that were dependent on reaction distance, increasing by more than 50% at the highest distances with respect to the established value. The only non-reproducibility of the results that has been observed was for the ratio of the flow through the injector to the flow of the carrier gas through the reactor, under turbulent flow conditions. A minimum of about 2×10^{-4} was necessary to get a reproducible value, implying that SO_2/N_2 mixtures flowing through the injector should have mole fractions lower than 1×10^{-3}.

The total range of pressure explored in the present study is 1.8–30.2 hPa with no effect on the rate constant values, as illustrated in Fig. 4. At room temperature, the average rate constant reported is $k_{10} = (1.08 \pm 0.11) \times 10^{-9}$ cm^3 molecule^{-1} s^{-1}, where the uncertainties are only statistical (2σ, 41 experiments). Other errors have been estimated to be 25%, including uncertainties of about 10% each for ion flow velocity, $[SF_6^-]/[SF_6^-]_0$ ratio, SO_2 dilution in the bulb, SO_2 flow, total gas flow in the tube, and average flow tube pressure. This results in overall uncertainties of 27%. The values at 298 K calculated from the classical trajectory collision theory by the model of Su [18] and the model of the average dipole orientation (ADO) [19,20] are 1.37×10^{-9} and 1.15×10^{-9} cm^3 molecule^{-1} s^{-1}, respectively, using the polarizability (3.72×10^{-24} cm^3) and the dipole moment (1.63 D) of SO_2 [27]. The difference with the experimental value is too small to

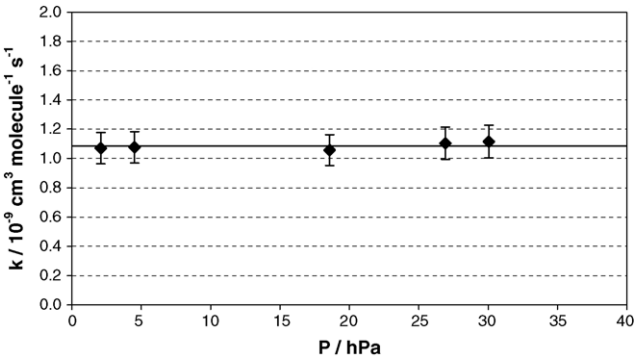

Fig. 4. Room temperature rate constant of the reaction $SF_6^- + SO_2$ as a function of pressure. Error bars represent only experimental scatter (2σ lead to 10% errors) and the solid line represents the average rate constant (1.08×10^{-9} cm^3 molecule^{-1} s^{-1}).

question the occurrence of the reaction by a single minimum of the potential surface (corresponding to only one intermediate stable complex). By contrast, the reactions of SF_6^- with O_3, Cl_2 and NO_2 proceed more slowly than collision theory predicts [23], due to a mechanism involving a double-well separated by an internal potential barrier [40]. Furthermore temperature has been varied between 240 and 373 K, and no significant variation of the rate constant was observed, which is consistent with the fact that the reaction studied proceeds by a single intermediate stable complex. Indeed, in the latter case collision theory applies and ADO theory calculations [19,20] result in a too slight rate constant variation (<0.2 $\times$ 10^{-9} cm^3 molecule^{-1} s^{-1}) in this temperature range to be detected experimentally, given the estimated uncertainties reported above (27%). On the contrary, rate constant variations may be observed in this temperature range for reactions with a double-well potential [40]. Owing to the good agreement between the experimental values and the ADO results, these one may be used to extrapolate variations over a larger temperature range.

A comparison of our result with all previous studies obtained at room temperature is given in Table 1. The excellent agreement between the previous studies has motivated the choice of this reaction, considered as a reference, and the new result obtained here supports this. The slight difference (10%) between the two more recent studies (including ours) conducted at higher pressures and the others at lower pressure is insignificant since our results also recover the low pressure domain. Moreover this shows the great interest to perform kinetic studies in the intermediate pressure range (2–50 hPa) not much explored for ion/molecule reactions studies. Variation of the rate constant in this pressure range may be significant for some association reactions and it is interesting to determine at which pressure the rate constant reaches its high pressure limit, which high pressure studies alone cannot probe.

Table 1
Comparison of the room temperature rate constant values obtained in this work with previous studies

k[a]	P (hPa)	Reference
1.1 ± 0.3	1.8–30.2	This work
1.1 ± 0.3	33–933	[22]
1.0 ± 0.3	<1.3	[45]
1.0 ± 0.3	0.5	[46]
1.0 ± 0.3	<1.7	[47]

[a] Units of 10^{-9} cm^3 molecule^{-1} s^{-1}. Reported uncertainties are global, including experimental scatter (2σ) and estimated systematic errors.

3.3. Product study

The product study was performed at low resolution of the mass analyzer to limit mass discrimination. Under these conditions, we have shown in a previous work that mass discrimination for ions of masses between 48 and 146 amu is usually lower than 20% [23]. Product ions detected in the present study having masses in a more restricted range, this gives the maximum systematic uncertainties associated with the branching ratios reported below, and no further correction was applied for mass discrimination. Good confidence in the results was reinforced by the mass balance obtained, defined by the ratio of the sum of the product ion count rates to the reactant ion (SF_6^-) consumption, which was generally equal to 100 ± 10%. This indicates that additional mass discrimination caused by the difference between the high pressure of the reactor and the low pressure of the first differentially pumped chamber is not important in the present experiments, a problem that may arise [41,42]. Reproducibility with respect to electrostatic conditions of ion focusing in the detection zone was also tested. In particular, variations of a factor of 10 of the potential difference applied between the sampling and skimmer conical electrodes of the first chamber resulted in no systematic dependence of the product distribution. The product ions therefore seem to be insensitive to collisions induced by the electric fields during sampling, focusing and detection. In order to minimize interferences with secondary reactions between the neutral reactant and the primary product ions of the title reaction, SO_2 flow was maintained low so that consumption of the SF_6^- was less than 20%. This usually led to good ($R^2 > 0.96$) linear correlations between the product ion count rates and the SF_6^- loss. This is a first method giving slopes that could be used for determining the product distribution after normalization of the mass balance to unit. However, for comparison purpose with previous studies, the branching ratios were determined by the standard method [43], i.e. by plotting the relative yields of the product ions as a function of SO_2 concentration and extrapolating the measured values to a null SO_2 flow to eliminate the effect of secondary reactions. A typical plot is shown in Fig. 5, leading to similar results as the first method.

The reaction was found to occur via three channels:

$$SF_6^- + SO_2 \rightarrow SO_2F_2^- + SF_4 \quad (11a)$$

$$\rightarrow SF_5^- + SO_2F \quad (11b)$$

$$\rightarrow SO_2F^- + SF_5 \quad (11c)$$

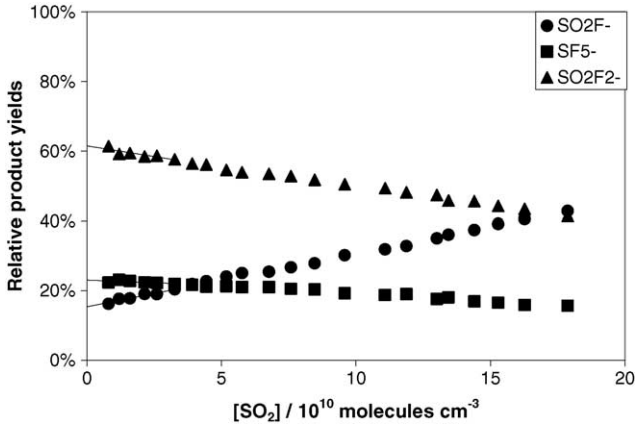

Fig. 5. Typical set of data (248 K, 20 hPa) used for determining product yields. Only the measurements at low SO_2 concentrations (<3.3×10^{10} molecules cm^{-3}) corresponding to SF_6^- consumption less than 20% were used for extrapolation to zero intercept.

The product yields were corrected for the presence of SF_5^- as reactant ion in traces. Results are summarized in Table 2. The global average yields are $57 \pm 16\%$ for $SO_2F_2^-$, $25 \pm 7\%$ for SF_5^-, and $18 \pm 5\%$ for SO_2F^-, where the quoted uncertainties are overall, including combination of estimated systematic errors (20%) and statistical errors of 20% (2σ) by the method of error propagation. No significant effect of pressure or temperature was observed over the ranges explored (2–20 hPa; 248–373 K), which is expected for this fast bimolecular exchange reaction [40,44]. These results are in perfect agreement with the product yields of previous studies at room temperature and at various pressures [22,45], the averages of which are 57% for $SO_2F_2^-$, 25% for SF_5^-, and 18% for SO_2F^-.

As the primary reaction further progresses, secondary reactions take importance. Decays of $SO_2F_2^-$ and SF_5^- count rates and increase of SO_2F^- count rates, illustrated for example in Fig. 5, show that these primary products further react with SO_2 to yield SO_2F^- as a final product. This result is consistent with previous studies [22,46], in which SF_5^- was observed to react with SO_2 to give $SO_2F_2^-$ (by difluoride transfer), which in turn reacts with SO_2 (by fluoride transfer), leading again to SO_2F^-. An additional very minor channel for the latter reaction may be

$$SO_2F_2^- + SO_2 \rightarrow (SO_2)_2F_2^- \quad (12)$$

since a secondary product at $m = 166$ amu, ascribed to $(SO_2)_2F_2^-$, was observed. We finally checked the possibility of reaction of SF_6 parent gas with the product ions $SO_2F_2^-$ giving again SF_5^-, as observed by Arnold et al. [22]. Variations of SF_6 concentrations injected into the flow tube by a factor of ten resulted in no discernable change for SF_5^- yield. This reaction is thus negligible under our experimental conditions, in which reaction times are sufficiently short that very slow reactions negligibly occur.

4. Conclusions

A new ion flow reactor has been set up for studying ion/molecule reactions in wide ranges of temperature (213–373 K) and pressure (1–50 hPa). This has been made possible by using laminar as well as turbulent flows, which showed properties in agreement with previous flow tube studies of ion and neutral species performed under various conditions [21,22,30,31,39]. In low pressure laminar regime ($Re < 1000$, $P < 7$ hPa), the average ion velocity has been found to be equal to the carrier gas velocity near the flow tube axis, but larger than the bulk flow velocity due to an ion radial concentration gradient. At higher flow rates ($Re > 2600$, $P > 15$ hPa), ion velocity and carrier gas velocities were found equal and constant across almost the flow tube diameter due to turbulent mixing.

This flow dynamics characterization has allowed to obtain consistent results for the reaction of SF_6^- with SO_2 in an intermediate pressure range (1.8–30.2 hPa) never explored until now. The rate constant and products measured at room temperature were indeed the same as those obtained in previous studies conducted at low (<2 hPa) or very high pressures (>30 hPa) [22,45–47]. In addition, the temperature dependence of the kinetics and mechanism for this reaction has been studied, leading to very consistent data over a wide range of experimental conditions in this new setup. This definitely establishes $SF_6^- + SO_2$ as a reference reaction for future fast flow reactors or reaction kinetics validation.

Finally, this validated experimental system can now be used to obtain data for a number of ion/molecule reactions in wide ranges of pressure and temperature. This will allow for the potential detection of a variety of atmospheric trace gases measured by this CIMS method, which is complementary to APCI-MS, which requires calibration standards, and to PTR-MS, which is essentially dedicated to organic molecules and unable to distinguish between compounds of same molecular mass.

Table 2
Products yields obtained in this work as a function of pressure and temperature

T (K)	2.1 hPa			20 hPa		
	SO_2F^- (%)	SF_5^- (%)	$SO_2F_2^-$ (%)	SO_2F^- (%)	SF_5^- (%)	$SO_2F_2^-$ (%)
248	15.1	22.3	62.5	16.0	23.7	60.3
296	15.7	26.1	58.2	19.0	24.7	56.4
373	20.1	25.3	54.6	23.9	24.9	51.2

Acknowledgements

The "Conseil Régional du Centre" is gratefully acknowledged for financial support. A. Kukui (Service d'Aéronomie-CNRS) is acknowledged for his fruitful comments on the manuscript.

References

[1] K.L. Foster, R.A. Plastridge, J.W. Bottenheim, P.B. Shepson, B.J. Finlayson-Pitts, C.W. Spicer, Science 291 (2001) 471.
[2] C. Warneke, C. van der Veen, S. Luxembourg, J.A. de Gouw, A. Kok, Int. J. Mass Spectrom. 207 (2001) 167.
[3] T. Karl, A. Hansel, T. Märk, W. Lindinger, D. Hoffmann, Int. J. Mass Spectrom. 223/224 (2003) 527.
[4] J. de Gouw, C. Warneke, T. Karl, G. Eerdekens, C. van der Veen, R. Fall, Int. J. Mass Spectrom. 223/224 (2003) 365.
[5] D. Smith, A.M. Diskin, Y. Ji, P. Spanel, Int. J. Mass Spectrom. 209 (2001) 81.
[6] G. Knop, F. Arnold, Geophys. Res. Lett. 14 (1987) 1262.
[7] F.L. Eisele, D.J. Tanner, J. Geophys. Res. 98 (D5) (1993) 9001.
[8] F. Arnold, V. Bürger, B. Droste-Fanke, F. Grimm, A. Krieger, J. Schneider, T. Stilp, Geophys. Res. Lett. 24 (1997) 3017.
[9] E.A. Arijs, A. Barassin, E. Kopp, C. Amelynck, V. Catoire, H.P. Fink, C. Guimbaud, U. Jenzer, D. Labonnette, W. Luithardt, E. Neefs, D. Nevejans, N. Schoon, A.-M. Van Bavel, Int. J. Mass Spectrom. Ion Process. 181 (1998) 99.
[10] L.G. Huey, E.J. Dunlea, E.R. Lovejoy, D.R. Hanson, R.B. Norton, F.C. Fehsenfeld, C.J. Howard, J. Geophys. Res. 103 (1998) 3355.
[11] J. Schneider, F. Arnold, V. Bürger, B. Droste-Franke, F. Grimm, G. Kirchner, M. Klemm, T. Stilp, K.-H. Wohlfrom, P. Siegmund, P.F.J. van Velthoven, J. Geophys. Res. 103 (1998) 25337.
[12] J.A. Neuman, R.S. Gao, M.E. Schein, S.J. Ciciora, J.C. Holecek, T.L. Thompson, R.H. Winkler, R.J. McLaughlin, M.J. Northway, E.C. Richard, D.W. Fahey, Rev. Sci. Instrum. 71 (2000) 3886.
[13] H. Berresheim, T. Elste, C. Plass-Dülmer, F.L. Eisele, D.J. Tanner, Int. J. Mass Spectrom. 202 (2000) 91.
[14] T.M. Miller, J.O. Ballenthin, R.F. Meads, D.E. Hunton, W.F. Thorn, A.A. Viggiano, Y. Kondo, M. Koike, Y. Zhao, J. Geophys. Res. 105 (2000) 3701.
[15] M. Hanke, B. Umann, J. Uecker, F. Arnold, H. Bunz, Atmos. Chem. Phys. 3 (2003) 417.
[16] A. Kiendler, F. Arnold, Int. J. Mass Spectrom. 223 (2003) 733.
[17] C. Jost, D. Sprung, T. Kenntner, T. Reiner, Int. J. Mass Spectrom. 223 (2003) 771.
[18] T. Su, J. Chem. Phys. 89 (1988) 5355.
[19] T. Su, M.T. Bowers, Int. J. Mass Spectrom. Ion Process. 17 (1975) 211.
[20] T. Su, M.T. Bowers, in: M.T. Bowers (Ed.), Gas Phase Ion Chemistry, vol. 1, Academic Press, New York, 1979, p. 83.
[21] J.V. Seeley, J.T. Jayne, M.J. Molina, Int. J. Chem. Kinet. 25 (1993) 571.
[22] S.T. Arnold, J.V. Seeley, J.S. Williamson, P.L. Mundis, A.A. Viggiano, J. Phys. Chem. 104 (2000) 5511.
[23] V. Catoire, C. Stépien, D. Labonnette, J.-C. Rayez, M.-T. Rayez, G. Poulet, Phys. Chem. Chem. Phys. 3 (2001) 193.
[24] J. Troe, J. Phys. Chem. 83 (1979) 114.
[25] W.B. DeMore, S.P. Sander, D.M. Golden, R.F. Hampson, M.J. Kurylo, C.J. Howard, A.R. Ravishankara, C.E. Kolb, M.J. Molina, Chemical Kinetics and Photochemical Data for Use in Stratospheric Modelling: Evaluation Number 12, Jet Propulsion Laboratory Publication 97-4, California Institute of Technology, Pasadena, 1997, p. 7.
[26] C. Guimbaud, D. Labonnette, V. Catoire, R. Thomas, Int. J. Mass Spectrom. 178 (1998) 161.
[27] D.R. Lide (Ed.), Handbook of Chemistry and Physics, 79th ed., CRC Press, Boca Raton, 1998.
[28] H. Schlichting, Boundary-Layer Theory, McGraw-Hill, New York, 1968.
[29] J.P.D. Abbatt, K.L. Demerjian, J.G. Anderson, J. Phys. Chem. 94 (1990) 4566.
[30] E.E. Ferguson, F.C. Fehsenfeld, A.L. Schmeltekopf, Adv. Atom. Mol. Phys. 5 (1969) 1.
[31] N.C. Adams, M.J. Church, D. Smith, J. Phys. D: Appl. Phys. 8 (1975) 1409.
[32] E.W. Mc Daniel, E.A. Mason, The Mobility and Diffusion of Ions in Gases, John Wiley & Sons, New York, 1973.
[33] R.C. Bolden, R.S. Hemsworth, M.J. Shaw, N.D. Twiddy, J. Phys. B: Atom. Mol. Phys. 3 (1970) 45.
[34] D. Smith, N.G. Adams, Adv. Atom. Mol. Phys. 24 (1988) 1.
[35] T.M. Miller, R.F. Wetterskog, J.F. Paulson, J. Chem. Phys. 80 (1984) 4922.
[36] B.L. Upschulte, R.J. Shul, R. Passarella, R.G. Keesee, A.W. Castleman, Int. J. Mass. Spectrom. Ion Process. 75 (1987) 27.
[37] J.A. de Gouw, M. Krishnamurthy, V.M. Bierbaum, S.R. Leone, Int. J. Mass. Spectrom. Ion Process. 167/168 (1997) 281.
[38] J. Baldyga, R. Pohorecki, Chem. Eng. J. 58 (1995) 183.
[39] S.C. Herndon, P.W. Villalta, D.D. Nelson, J.T. Jayne, M.S. Zahniser, J. Phys. Chem. 105 (2001) 1583.
[40] C.R. Moylan, J.I. Brauman, in: W.L. Hase (Ed.), Advances in Classical Trajectory Methods, vol. 2, JAI Press Inc., London, 1994, p. 95.
[41] D.R. Zook, E.P. Grimsrud, J. Am. Soc. Mass Spectrom. 2 (1991) 232.
[42] J.K. Hovey, A. Likholyot, Int. J. Mass Spectrom. 202 (2000) 147.
[43] N.G. Adams, D. Smith, J. Phys. B: Atom. Mol. Phys. 9 (1976) 1439.
[44] M. Meot-Ner, in: M.T. Bowers (Ed.), Gas Phase Ion Chemistry, vol. 1, Academic Press, New York, 1979, p. 197.
[45] L.G. Huey, D.R. Hanson, C.J. Howard, J. Phys. Chem. 99 (1995) 5001.
[46] G.E. Streit, J. Chem. Phys. 77 (1982) 826.
[47] E.E. Ferguson, Int. J. Mass Spectrom. Ion Phys. 19 (1976) 53.